PHYSICAL REVIEW C **93**, 064607 (2016)

Backscattering measurement of ^{6}He on ^{209}Bi: Critical interaction distance

V. Guimarães,[1,2] J. J. Kolata,[3] E. F. Aguilera,[4] A. Howard,[3] A. Roberts,[3] F. D. Becchetti,[5] R. O. Torres-Isea,[5] A. Riggins,[5] M. Febrarro,[6] V. Scarduelli,[1] P. N. de Faria,[7] D. S. Monteiro,[8] J. F. P. Huiza,[9] A. Arazi,[10] J. Hinnefeld,[11] A. M. Moro,[12] E. S. Rossi Jr.,[13] V. Morcelle,[14] A. Barioni,[15] and Alan J. Mitchell[16]

[1]*Instituto de Física, Universidade de São Paulo, Travessa R da Rua do Matao 187, 05508-900 São Paulo, São Paulo, Brazil*
[2]*Institute de Physique Nucleaire (IPN) d'Orsay, 15 Rue Georges Clemenceau 91406 Orsay, France*
[3]*Physics Department, University of Notre Dame, Notre Dame, Indiana 46556-5670, USA*
[4]*Departamento de Aceleradores del Instituto Nacional de Investigaciones Nucleares, Apartado Postal 18-1027 Codigo Postal 11801, Mexico, Distrito Federal, Mexico*
[5]*Physics Department, University of Michigan, Ann Arbor, Michigan 48109-1040, USA*
[6]*University of Tenneessee, Knoxville, Teneessee, USA*
[7]*Instituto de Física da Universidade Federal Fluminense, Avenida Litoranea s/n, Gragoata, Niteroi, Rio de Janeiro 24210-340, Brazil*
[8]*Universidade Federal da Integração Latino-Americana, Instituto Latino-Americano de Ciências da Vida e da Natureza, Foz do Iguaçu, Paraná, Brazil*
[9]*Universidade Estadual do Sudoeste da Bahia, Bahia, Brazil*
[10]*Laboratorio Tandar da Comision Nacional de Energia Atomica, B1650KNA San Martin, Buenos Aires, Argentina*
[11]*Department of Physics and Astronomy, Indiana University at South Bend, South Bend, Indiana 46634, USA*
[12]*Departamento de FAMN, Universidad de Sevilla. Apartado 1065, 41080 Sevilla, Spain*
[13]*UNIFIEO-Centro Universitario FIEO-CEP 06020-190, Osasco-SP, Brazil*
[14]*Departament of Physics, Universidade Federal Rural do Rio de Janeiro, Seropédica, 23890-000 Rio de Janeiro, Brazil*
[15]*Instituto de Física, Universidade Federal da Bahia, 40210-340, Salvador, Bahia, Brazil*
[16]*Department of Nuclear Physics, Australian National University, Canberra, ACT 2601, Australia*

(Received 16 January 2016; revised manuscript received 2 May 2016; published 14 June 2016; corrected 28 June 2016)

An elastic backscattering experiment has been performed at energies below the Coulomb barrier to investigate static and dynamic effects in the interaction of ^{6}He with ^{209}Bi. The measured cross sections are presented in terms of the $d\sigma/d\sigma_{Ruth}$ ratio, as a function of the distance of closest approach on a Rutherford trajectory. The data are compared with a three-body CDCC calculation and good agreement is observed. In addition, the critical distance of interaction was extracted. A larger value was obtained for the exotic ^{6}He nucleus as compared with the weakly bound ^{6}Li and ^{9}Be nuclei and the tightly bound ^{4}He, ^{12}C, and ^{16}O nuclei.

DOI: 10.1103/PhysRevC.93.064607

I. INTRODUCTION

A considerable amount of effort has been devoted in the past 15 years to investigating the influence of the anomalous *borromean* configuration of the ^{6}He nucleus on several different reaction mechanisms. In ^{6}He, the valence dineutron is weakly bound in a predominant S state to the ^{4}He core, with a separation energy $S_{2n} = 0.975$ MeV. Such a configuration favors the development of a very diffuse neutron surface layer, as opposed to ordinary nuclei which have a more well-defined radius. The exotic geometric (static) effect of this nucleus is found to strongly influence the dynamics of ^{6}He-induced reactions [1]. In this work we investigate these static and dynamic effects by using elastic-scattering measurements. Elastic scattering is the simplest process which can occur in the collision of two nuclei, and at low energies it is the process with the largest cross section. This is a relevant feature for experiments with radioactive ion beams which usually have intensities six orders of magnitude lower than stable beams. The analysis of the elastic scattering angular distributions, measured at energies not too far from the Coulomb barrier, can thus provide valuable information on static and dynamic effects of exotic nuclei. It is well known that sub-barrier elastic scattering of stable projectiles should follow the Rutherford law. However, elastic cross sections for exotic nuclei such as ^{11}Li can deviate significantly from pure Rutherford scattering even at rather far sub-barrier energies [2].

Many elastic-scattering measurements using the radioactive ^{6}He projectile on several medium- to heavy-mass targets have been performed in the last 15 years, and they were reviewed in Refs. [3,4]. Among them we can cite: ^{6}He + ^{209}Bi [5], ^{6}He + ^{208}Pb [6–8], ^{6}He + ^{64}Zn [9], ^{6}He + ^{27}Al [10], ^{6}He + ^{120}Sn [11], and more recently ^{6}He + ^{9}Be [12] and ^{6}He + ^{58}Ni [13,14]. These experiments have shown the importance of the static and dynamic effects originating from the borromean configuration and extended mass distribution as well as due to the weak binding energy of ^{6}He. For instance, in terms of three-body (n-n-α) and two-body ($2n$-α) cluster models for ^{6}He, which relate to a static effect, we would expect that the three-body model would give a better description of the data. However, elastic scattering angular distributions for ^{6}He + ^{58}Ni [13] and ^{6}He + ^{208}Pb [8] are better described by the simplified two-body ($2n$-α) calculations. In Ref. [15], angular distributions for ^{6}He + ^{209}Bi at forward angles are better described by the three-body CDCC calculation while backward angles are better described by a two-body model. Moro *et al.* demonstrated in Ref. [16] that the use of 1.6 MeV as the separation energy for ^{6}He, instead of 0.973 MeV, provided results for the three-body calculation

that are closer to the two-body values. In terms of dynamic effects, the low binding of ^{6}He makes it prone to breakup, even in the long-range Coulomb field of the target. It is then expected that the dipole component of the Coulomb interaction would play an important role in coupling to the continuum at energies close to the barrier, especially since ^{6}He has a high dipole polarizability (1.2 fm^{3}). The ^{6}He $+^{208}$Pb elastic scattering data from Ref. [7] was better described by including a Coulomb dipole potential (CDP) in the calculation. However, it was found that this CDP was only partly responsible for the long range absorption, and the authors claimed that other reaction channels could also produce absorption at large distance. In most of the ^{6}He elastic-scattering references, introduction of a long-range component into the absorptive potential was necessary to describe the data. This long-range absorption, responsible for the loss of elastic flux, could be the combination of effects related to both the nuclear and Coulomb interaction, and/or interference between them. The origin and characteristics of this long-range component is yet to be fully understood. The transfer channels, usually ignored in most CDCC calculation, can be important in the coupling scheme and this has not been fully explored. As mentioned by Keeley, *et al.* in Ref. [17], the coupling to transfer channels can drastically change the barrier distribution for elastic scattering measured at backward angles.

In the present experiment, we aim to investigate the effect of the long range absorption through the determination of the phenomenological interaction distance from a backscattering cross section measurement below Coulomb barrier. Since it is a surface process, backscattering can be a powerful tool to study the surface properties of the nucleus-nucleus potential in heavy-ion reactions [18,19]. At backward angles, a stronger interaction between peripheral scattering from the repulsive Coulomb potential and the influence of the absorptive nuclear interaction is expected, due to the extended diffuse surface region of the ^{6}He nucleus. The present measurement reduces the statistical uncertainties in the cross section at backward angles of a previous experiment [5] with the same system.

The outline of the paper is as follows. In Sec. II, experimental details about the new measurements for the backscattering of ^{6}He $+^{209}$Bi are presented. In Sec. III, the procedure used to obtain the critical interaction distance is explained, and the values obtained for ^{6}He data on heavy targets are given and compared with values from other systems. The final discussion and conclusions are given in Sec. IV.

II. EXPERIMENTAL DETAILS AND SETUP

The measurements for the elastic backscattering of ^{6}He on ^{209}Bi were performed at three energies below the Coulomb barrier ($E_{\rm lab} = 12$, 14, and 16 MeV), in two different runs at backward angles between $110^{\circ} < \theta_{\rm lab} < 150^{\circ}$. Forward angle measurements at $\pm 30^{\circ}$ were also performed for normalization purposes. A small correction factor, due to possible small error in the determination of the energy and/or solid angles, was necessary to normalize the cross section to Rutherford at 12 MeV. The same normalization factor was then used for the 14 and 16 MeV data. The secondary ^{6}He radioactive beam was obtained from the *TwinSol* facility at the Nuclear Structure Laboratory of the University of Notre Dame, USA [20]. In this case, the beam was produced in a primary target via the ^{2}H(^{7}Li ,^{6}He) reaction. The primary ^{7}Li beam had an energy of 32 MeV, an average intensity of 1 eμA, and was accelerated by a 9.5 MV tandem Van de Graaff accelerator. The production target consisted of a gas cell 2.5 cm long filled with ^{2}H gas at a pressure of 1 atm. The windows of the gas cell consisted of 2 μm thick Havar foils. The two superconducting solenoids in the *TwinSol* system act as thick lenses to collect, select, and focus the secondary beam into a scattering chamber. The ^{6}He beam had an average intensity of 5.0×10^{5} particles per second per 1 eμA of primary beam with an energy resolution of $\approx$0.450 MeV (FWHM), determined from the elastic scattering measurements at forward angles. The beam was focused onto a 4.3 mg/cm^{2} thick ^{209}Bi secondary target. Previous to the scattering measurement, the flux in the secondary beam was checked by inserting a silicon ΔE-E telescope at the secondary target position and reducing the intensity of the primary beam by 3 orders of magnitude, in such a way that the ^{6}He particles could be directly counted while at the same time the primary beam current was measured in a Faraday cup. Some beam contamination with ions having the same magnetic rigidity as the ^{6}He beam was also present. This contamination was reduced by placing an 8 μm Havar foil at the crossover point between the two solenoids. Differential energy loss then helps to eliminate unwanted ions from the beam prior to the secondary bismuth target. The purity of the ^{6}He beam was then $\approx$90% and the remaining contaminant ^{4}He ions could be identified and did not interfere with the elastic data since they had a very different energy. The beam profile measurement at zero degrees is shown in Fig. 1.

In the first run, scattered particles were detected with four telescopes placed at laboratory angles of 130, 140, 150, and 160 degrees, while in the second run seven Si ΔE-E telescopes were placed at backwards angles between 110 and 150 degrees on either side of the beam. Each of these telescopes had a circular collimator that subtended a solid angle of about 10 msr, corresponding to an effective angular resolution of 6°. Two telescopes, with smaller collimators, 2.3 msr in the first run and 0.7 msr in the second, were placed at $\pm$30 degrees for normalization purposes.

III. CROSS SECTIONS AS A FUNCTION OF INTERACTION DISTANCE

A phenomenological investigation of the influence of the static effect of the exotic properties of ^{6}He can be performed by plotting the ratio of the elastic cross section to the Rutherford value, $d\sigma/d\sigma_{Ruth}$, as a function of the distance of closest approach D on a classical Rutherford trajectory [21]. This distance is related to the incident energy and the scattering angle θ in the center of mass frame as follows:

$$D = \frac{1}{2} D_0 \left(1 + \frac{1}{\sin(\theta_{\rm c.m.}/2)} \right) \tag{1}$$

with

$$D_0 = \frac{Z_P Z_T e^2}{E_{\rm c.m.}} \tag{2}$$

being the distance of closest approach in a head-on collision.

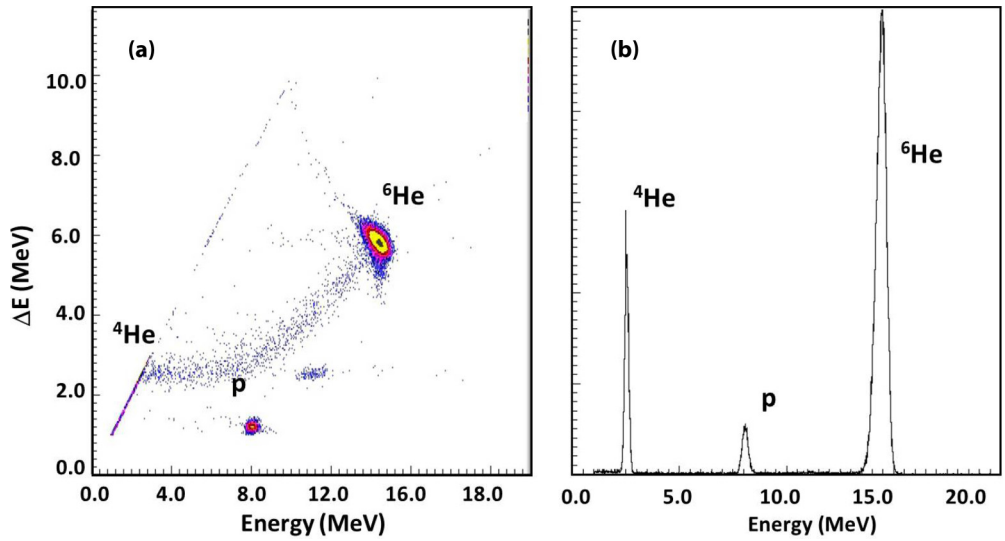

FIG. 1. The ΔE-E spectra for the ^{6}He beam at 14 MeV.

To describe the method applied here, consider the $d\sigma/d\sigma_{Ruth}$ ratio plot as a function of reduced distance of closest approach $d = D/(A_P^{1/3} + A_T^{1/3})$ for the ^{16}O + ^{209}Bi system shown in Fig. 2. The elastic scattering data for this system were obtained from Ref. [22]. As observed in the figure, the $d\sigma/d\sigma_{Ruth}$ ratio is close to unity for larger distances but falls off very rapidly at short distances due to strong absorption of the elastic flux by non-elastic channels (mostly fusion for this system). The nuclear surface effect appears between the two regions. Following Pakou and Rusek [21], the critical interaction distance (D_I) is defined as the distance at which the ratio of elastic scattering to the Rutherford cross section drops to 0.98 or, in other words, where the absolute value of the S matrix = 0.99. As in this reference, the reduced critical interaction distances, d_I, were obtained by fitting the corresponding elastic data as a function of the reduced distance of closest approach with a Boltzmann-type exponential function:

$$y = \frac{p_1}{1 + e^{d_1 * (d - d_2)}}, \tag{3}$$

where y is the $d\sigma/d\sigma_{Ruth}$ ratio, d is the reduced distance of closest approach, and p_1,d_1 and d_2 are adjustable parameters. This expression is used here not because it has any real physical meaning for elastic scattering but rather because it provides a good fit to the data in the region of interest and therefore enables the extraction of d_I in a consistent and uniform manner. The reduced critical interaction distance obtained for the ^{16}O + ^{209}Bi system is $d_I = 1.63 \pm 0.01$ fm corresponding to a distance $D_I = 13.78 \pm 0.08$ fm. This distance is not so far from the classical grazing distance $R = 1.3 \times (A_P^{1/3} + A_T^{1/3}) = 10.99$ fm for this system. The strong-absorption distance, which corresponds to the point where the ratio of elastic scattering to Rutherford drops to 0.25 ($|S| = 0.5$) is found to be $d_S = 1.493 \pm 0.002$ or $D_S = 12.66 \pm 0.02$ fm for this system. This is the point where the elastic scattering is most sensitive to the values of the optical-model nuclear potential parameters.

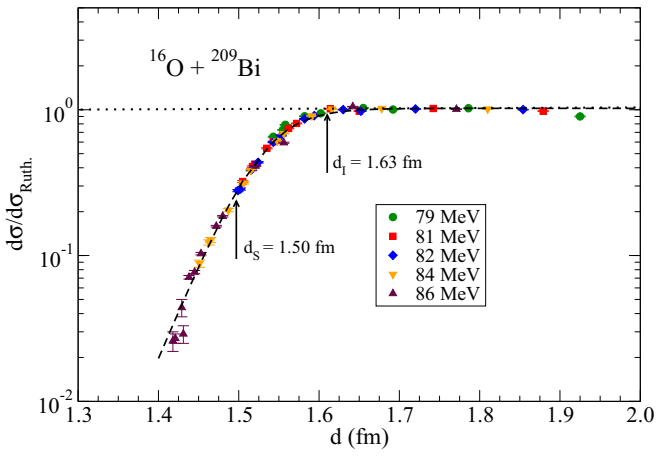

FIG. 2. Ratio of elastic to Rutherford cross sections, $d\sigma/d\sigma_{Ruth}$, as a function of the reduced distance of closest approach d for the ^{16}O + ^{209}Bi system. The data on elastic scattering were obtained from Ref. [22]. The dashed curve corresponds to a fit with an exponential function as explained in the text.

The σ/σ_{Ruth} ratio plot as a function of the distance of closest approach D for the ^{6}He + ^{208}Pb system is shown in Fig. 5 of Ref. [7]. However, these data do not completely cover the important transitional region between 15–22 fm and the points lying the region between 18–22 fm are exclusively from measurements at forward angles. Another elastic scattering measurement for the ^{6}He + ^{208}Pb system has been performed at E_{lab} = 22 MeV [8]. This experiment covered a larger range of forward angles but also included the same backward-angle region as in the work of Sánchez-Benítez [7]. Since we did not initially expect much difference between ^{6}He + ^{209}Bi and ^{6}He + ^{208}Pb, we decided to investigate this transitional region using measurements only at backward angles. The results for the cross sections at all the energies and angles measured in the present work are illustrated in Fig. 3. As can be seen, these data cover the distance region from 15 to 22 fm, which corresponds to d = 2.0 to 3.0 fm.

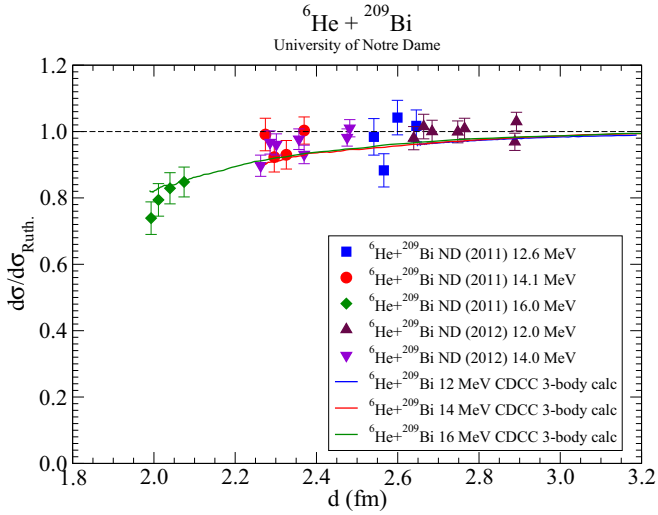

FIG. 3. Ratio of elastic to Rutherford cross sections, $d\sigma/d\sigma_{Ruth}$, as a function of the reduced distance d for the ^{6}He + ^{209}Bi system (present work). Data taken in the various runs are indicated. The solid lines correspond to CDCC calculations explained in the text.

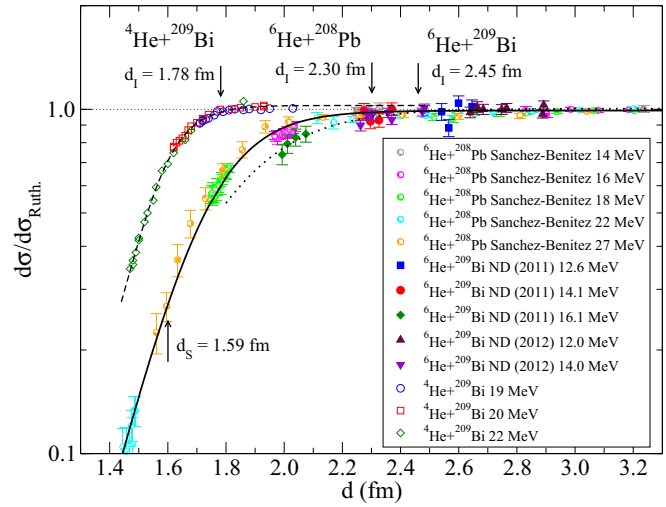

FIG. 4. Ratio of elastic to Rutherford cross sections, $d\sigma/d\sigma_{Ruth}$, as a function of the reduced distance d for the systems and energies indicated. The data on elastic scattering for ^{4}He + ^{209}Bi were obtained from Ref. [24] and for ^{6}He + ^{208}Pb from Ref. [7]. The curves correspond to fits with exponential functions as explained in the text.

A. CDCC calculations

The solid curves in Fig. 3 correspond to a three-body continuum discretized coupled-channel (CDCC) calculation [23] using a simple dineutron model for the ^{6}He nucleus (developed in Ref. [16]). This model assumes that the ^{6}He ground state is described by a $2n$-^{4}He two-body model, with an effective two-neutron separation energy of $S_{2n} = 1.6$ MeV and a pure $2S$ configuration. The $2n$-^{4}He interaction was parametrized in terms of a Woods-Saxon potential with radius $R = 1.9$ fm and diffuseness $a = 0.39$ fm. To generate the continuum states, partial waves $\ell = 0$, 1, and 2 were considered. The potential for $\ell = 0$ had the same geometry and depth as in the ground state (g.s.). For $\ell = 2$ the same geometry was used but the depth was adjusted to obtain the 2^+ resonance at the correct excitation energy with respect to the g.s. This same depth was used for the $\ell = 1$ continuum states, again using the g.s. geometry. In the calculation, a maximum value for the total angular momentum of $J_{max} = 150$, and a maximum integration radius of 80 fm were used. The α-target and $2n$-target interactions, necessary to generate the ^{6}He-target coupling potentials, were represented by optical-model potentials evaluated at the appropriate energy. We used the Barnett and Lilley potential [24] for $\alpha + ^{209}$Bi. The $2n + ^{209}$Bi potential was calculated by folding the sum of the $n + ^{209}$Bi optical model potentials, obtained from the Koning-Delaroche [25], with a neutron-neutron density function. The latter was obtained from a three-body calculation of ^{6}He. Further details can be found in Ref. [12]. Four-body CDCC calculations are feasible for this system [26] but it has been shown that three-body CDCC calculations, using an adequate two-body cluster model for ^{6}He, are able to reproduce the elastic data quite well [16]. For simplicity, the latter was adopted for the present calculations. As one can see, the calculation describes fairly well the overall trend of the experimental data given that no free parameters were fitted.

B. Critical interaction distance

As mentioned, the $d\sigma/d\sigma_{Ruth}$ ratio as a function of the distance of closest approach is near unity for large distances. However, for distances smaller than a certain critical distance the two colliding nuclei are close enough so that the projectile begins to experience an interaction that absorbs flux from the elastic channel.

To obtain and compare the critical interaction distance for several different systems we removed the dependence on their size by considering the $d\sigma/d\sigma_{Ruth}$ ratio data as a function of the reduced distance of closest approach. The reduced critical interaction distances, d_I, were obtained by fitting the corresponding elastic data as a function of the reduced distance of closest approach with the Boltzmann-type exponential function described earlier.

The results of this fitting procedure considering data for the ^{4}He + ^{209}Bi system (Ref. [24]), the ^{6}He + ^{209}Bi system (this work), and the ^{6}He + ^{208}Pb system (Ref. [7]) are shown in Fig. 4. The critical interaction distance d_I at which the cross section is 0.98 of Rutherford was determined from these fits.

The data from the literature were converted from $d\sigma/d\sigma_{Ruth}$ as a function of angle for a given energy to $d\sigma/d\sigma_{Ruth}$ as a function of the distance of closest approach, without any additional normalization. All parameters in Eq. (3) were free to vary during the fitting procedure. The parameter p_1 in Eq. (3) is actually the asymptotic value of y for large distance d. This parameter is then associated to the normalization of the data, which should be close to the unity for large values of d. To take into account the data normalization, we also considered the reduced critical interaction distance, d_I^N, for which the $d\sigma/d\sigma_{Ruth}$ ratio is $0.98 \times p_1$.

The observed values for d_I and d_I^N, are listed in Table I together with the values obtained for some other data on a ^{209}Bi target available in the literature: ^{9}Be + ^{209}Bi from

TABLE I. The reduced critical interaction distance, d_I, at which $d\sigma/d\sigma_{Ruth} = 0.98$ for the systems indicated. The values d_I^N correspond to the distances with data normalization as discussed in the text. The predominant cluster configuration of the projectile and corresponding binding energy are also listed.

System	Reference	Cluster config.	B.E. (MeV)	d_I (fm)	d_I^N (fm)
^{4}He +^{209}Bi	Barnett-74 [24]	$t + p$	19.813	1.78 ± 0.02	1.86 ± 0.02
^{6}He +^{209}Bi	this work	^{4}He +2n	0.973	2.45 ± 0.16	2.50 ± 0.16
^{6}He +^{208}Pb	Sanchez-Benitez-08 [7]	^{4}He +2n	0.973	2.30 ± 0.20	2.23 ± 0.20
^{6}Li +^{209}Bi	Santra-11 [28]	^{4}He +d	1.474	1.96 ± 0.05	1.94 ± 0.05
^{9}Be +^{209}Bi	Yu-10 [27]	^{4}He +^{4}He+n	1.574	1.84 ± 0.02	1.86 ± 0.02
^{12}C +^{209}Bi	Santra-99 [29]	^{4}He +^{8}Be	7.367	1.65 ± 0.01	1.66 ± 0.01
^{16}O +^{209}Bi	Vulgaris-86 [22]	^{4}He +^{12}C	7.162	1.63 ± 0.01	1.66 ± 0.01

Ref. [27], ^{6}Li +^{209}Bi from Ref. [28], and ^{12}C +^{209}Bi from Ref. [29]. As one can see, the values with and without data normalization are a little bit different for ^{4}He and ^{6}He systems, but not enough to change the qualitative discussion along the paper. The uncertainties in these values were obtained by converting the uncertainty in the cross section ratios, when they were 0.98, to the uncertainty in distance. The uncertainty in the cross section ratios was taken to be one-half of the difference from where the ratios were 0.97 and 0.99. This is reasonable for the data of ^{4}He, ^{6}Li, ^{9}Be, ^{12}C, and ^{16}O projectiles which had a small experimental spread in the region of the critical interaction distance. However, to take into account the higher experimental uncertainty (3% on average) of the data for ^{6}He +^{209}Bi and ^{6}He +^{208}Pb, we used the variation of the distance when the ratios of the cross sections were between 0.96 and 1.00. To check the energy dependence of the critical interaction distance we performed a more detailed analysis on data for ^{9}Be +^{209}Bi, considering the seven angular distributions obtained from $E_{\rm lab}$ = 38.2 to 41.0 MeV. The first step was to fit each angular distribution by the Boltzmann-type exponential function to obtain the corresponding critical interaction distance for each energy. A very small energy dependence of the critical interaction distance, from $d_I = 1.874$ fm for $E_{\rm lab} = 38.2$ MeV to $d_I = 1.813$ fm for $E_{\rm lab} = 41.0$ MeV, was observed. Averaging the values derived for each angular distribution we obtained $\langle d_I \rangle = 1.84 \pm 0.03$ fm. The second step was to consider all data from the seven angular distributions together in the fitting procedure. The obtained critical interaction distance with all data together was $d_I = 1.84 \pm 0.02$ fm for the ^{9}Be +^{209}Bi system, which is in good agreement with the values obtained from the average of the values for each angular distribution. The fit to the total data set for this system can be seen in Fig. 5, together with the data set from ^{12}C +^{209}Bi [29].

The reduced critical interaction distance for ^{6}Li and ^{12}C projectiles can be compared with results obtained for ^{6}Li +^{208}Pb and ^{12}C +^{209}Bi by Pakou *et al.*, in Ref. [21]. They have performed a similar study for these two systems. By averaging their values, from Fig. 5 of their paper, we obtained $\langle d_I \rangle = 1.93 \pm 0.03$ and $\langle d_I \rangle = 1.64 \pm 0.01$ for ^{6}Li and ^{12}C, respectively, which are in a very good agreement with the values we obtained. We should emphasize, however, that their criteria to obtain the critical interaction distance is when the ratio of the cross section to Rutherford drops to 0.97.

The values with and without data normalization are a little bit different for ^{4}He and ^{6}He systems, but not enough to change the qualitative discussion along the paper.

The value $d_I = 2.45 \pm 0.16$ fm obtained for ^{6}He +^{209}Bi is quite large. This value would correspond to a distance $D_I = 18.91$ fm which is much larger than the grazing distance $R = R_P + R_T = 1.3 \times (A_P^{1/3} + A_T^{1/3}) = 10.08$ fm for this system. This value agrees well with the value deduced from the ^{6}He +^{208}Pb data set of Ref. [7]. The small difference for the two system could be an indication that the nuclear interaction may be different for these two systems. Based on the measurements at 16 MeV, the elastic scattering data for ^{6}He +^{209}Bi seem to fall a bit faster from Rutherford than in the ^{6}He +^{208}Pb case (Fig. 4). If verified, this difference could result from a structure effect such as the location of specific nuclear states within the corresponding Q windows for 1n and 2n transfer.

For the ^{6}He +^{208}Pb data we could also derive the reduced strong-absorption distance, d_s (where the ratio-to-Rutherford is 0.25), which is 1.59 ± 0.01 fm. It is interesting to note that this value is not so different from the value 1.493 ± 0.002 fm obtained for ^{16}O +^{209}Bi. Here the uncertainties for the reduced

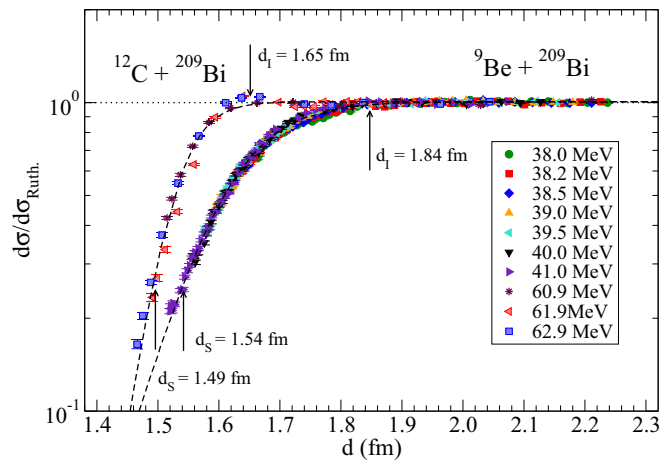

FIG. 5. Ratio of elastic to Rutherford cross sections, $d\sigma/d\sigma_{Ruth}$, as a function of the reduced distance d for the systems and energies indicated. The data on elastic scattering for ^{9}Be +^{209}Bi were obtained from Ref. [27] and for the ^{12}C +^{209}Bi from Ref. [29]. The curves correspond to the fits with exponential functions as explained in the text.

strong interaction distance were adopted by considering the variation of the cross section from 0.24 to 0.26 for ^{16}O and 0.23 to 0.27 for ^{6}He. The difference between the reduced strong-absorption distance and the reduced critical interaction distance, $\delta = d_I - d_S$, is 0.14 fm for ^{16}O and 0.82 fm for ^{6}He. In the region between these two radii, the main source of absorption of the elastic flux is a direct process (breakup, transfer, etc.). The extended region between the strong absorption distance and the critical interaction distance for the ^{6}He projectile indicates a longer-range influence of direct processes due to the more diffuse and extended surface of ^{6}He and effects of the Coulomb interaction and/or a long-range nuclear interaction.

The importance of breakup in describing the characteristic elastic angular distributions could be assessed in two ways. First by the importance of CDCC calculations in describing the data as discussed in the previous section and also in Ref. [15] for ^{6}He $+^{209}$Bi at 19 and 22.5 MeV, and secondly by a correlation between the breakup threshold for different projectiles and the critical interaction distance. Here, the breakup threshold corresponds to the binding energy of the cluster configurations shown in Table I. As can be seen in this table, the systems with the exotic ^{6}He nucleus as projectile have a larger critical interaction distance when compared with the values, e.g., for weakly bound ^{6}Li and ^{9}Be and tightly bound ^{4}He, ^{12}C, and ^{16}O nuclei. In the case of the two strongly-bound systems ^{12}C and ^{16}O, which have very similar binding energies, the critical interaction distances are basically identical. The two weakly bound systems ^{6}Li and ^{9}Be also have similar breakup threshold energies and their critical interaction distances agree within the uncertainties. This could be interpreted as a possible correlation between the importance of the breakup threshold and the corresponding critical interaction distance, and it deserves further investigation with other systems.

By comparing the values of critical interaction distance for ^{6}He with those for ^{6}Li and ^{4}He we can draw some conclusions. Comparing the critical interaction distance for ^{6}He and ^{4}He, there is clearly a larger interaction for the more diffuse-surface ^{6}He nucleus, which can be interpreted as due to several effects including the static extended-matter distribution and cluster configuration, as well as dynamic effects such as a lower breakup threshold inducing couplings to direct channels. The interesting comparison is between the values for ^{6}He and ^{6}Li. The Coulomb interaction is known to have a strong dynamic effect in nuclei with low breakup threshold as is the case for both ^{6}He and ^{6}Li (0.973 MeV and 1.474 MeV, respectively). However, since the electric dipole transition strengths for ^{6}Li are near zero due to its predominant $\alpha + d$ cluster configuration, whose effective charge is zero, and the dipole excitation mode for ^{6}He is found to be very high [30,31], the comparison of their elastic data can provide interesting information on the Coulomb interaction. Such a comparison has been performed and reported in Ref. [1] for the elastic scattering of ^{6}Li and ^{6}He on a ^{208}Pb target. It is evident in this work that the effect of the dipole polarizability is to lower the elastic scattering cross section at small angles, as also observed for ^{11}Li [2]. Here, the larger critical interaction distance observed for ^{6}He as compared to ^{6}Li could be an indication that dipole polarizability may be playing a very important role for ^{6}He systems.

IV. SUMMARY

We have measured the elastic backscattering of ^{6}He $+^{209}$Bi at three energies below the Coulomb barrier, $E_{\rm lab} = 12, 14$, and 16 MeV. The measurements were performed in two different runs at backward angles between $110^\circ < \theta_{\rm lab} < 160^\circ$. The results are displayed in terms of the ratio $\mathrm{d}\sigma/\mathrm{d}\sigma_{Ruth}$, as a function of the distance of closest approach on a Rutherford trajectory, and the data compared with three-body CDCC calculations. Good agreement is observed.

We extracted the critical interaction distance from the elastic data. A larger value of the interaction distance was observed for the exotic ^{6}He nucleus as compared with the weakly bound ^{6}Li and ^{9}Be nuclei and even more so when compared with the tightly bound ^{4}He, ^{12}C, and ^{16}O projectiles. The significantly larger value obtained for ^{6}He can be understood as due to the influence of long-range Coulomb couplings, mostly stemming from the large Coulomb dipole polarizability of this nucleus. These couplings, along with the low binding energy of this nucleus, are also responsible for the large transfer/breakup probabilities observed experimentally. Although existing reaction frameworks (such as the CDCC method used here) have been found to account very well for the effect of these couplings on the elastic scattering, a detailed account of the observables coming from transfer/breakup of ^{6}He and other three-body systems is still a challenging problem for nuclear reaction theories.

ACKNOWLEDGMENTS

The author V.G. would like to thank the São Paulo Research Foundation (FAPESP) (Grant No. 2014/14432-2) and the Conselho Nacional de Desenvolvimento Científico (CNPq) (Grant No. 302969/2013-6) for the financial support. V.M. thanks FAPERJ and D.S.M. thanks CNPq for financial support. A.M.M. is partially supported by the Spanish Ministerio de Economía y Competitividad, under grants no. FIS2013-41994-P and FIS2014-53448-C2-1-P. This work was partially supported by the U.S. National Science Foundation under Grants No. PHY14-01343 and PHY14-01242 and by CONACYT (Mexico).

[1] K. Rusek, N. Keeley, K. W. Kemper, and R. Raabe, Phys. Rev. C **67**, 041604(R) (2003).

[2] M. Cubero *et al.*, Phys. Rev. Lett. **109**, 262701 (2012).

[3] N. Keeley, N. Alamanos, K. W. Kemper, and K. Rusek, Prog. Part. Nucl. Phys. **63**, 396 (2009).

[4] J. J. Kolata, V. Guimarães, and E. F. Aguilera, Eur. Phys. J. A **52**, 123 (2016).

[5] E. F. Aguilera *et al.*, Phys. Rev. C **63**, 061603(R) (2001).
[6] O. R. Kakuee *et al.*, Nucl. Phys. A **728**, 339 (2003).
[7] A. M. Sánchez-Benítez *et al.*, Nucl. Phys. A **803**, 30 (2008).
[8] L. Acosta *et al.*, Phys. Rev. C **84**, 044604 (2011).
[9] A. Di Pietro *et al.*, Phys. Rev. C **69**, 044613 (2004).
[10] E. A. Benjamin *et al.*, Phys. Lett. B **647**, 30 (2007).
[11] P. N. de Faria, *et al.*, Phys. Rev. C **81**, 044605 (2010).
[12] K. C. C. Pires *et al.*, Phys. Rev. C **83**, 064603 (2011).
[13] V. Morcelle *et al.*, Phys. Lett. B **732**, 228 (2014).
[14] L. R. Gasques *et al.*, Phys. Rev. C **67**, 024602 (2003).
[15] T. Matsumoto, T. Egami, K. Ogata, Y. Iseri, M. Kamimura, and M. Yahiro, Phys. Rev. C **73**, 051602(R) (2006).
[16] A. M. Moro, K. Rusek, J. M. Arias, J. Gòmez-Camacho, and M. Rodríguez-Gallardo, Phys. Rev. C **75**, 064607 (2007).
[17] N. Keeley, Phys. Rev. C **80**, 064614 (2009).
[18] K. Washiyama, K. Hagino, and M. Dasgupta, Phys. Rev. C **73**, 034607 (2006).
[19] K. Zerva *et al.*, Eur. Phys. J. A **48**, 102 (2012).
[20] F. D. Becchetti *et al.*, Nucl. Instrum. Methods Res. A **505**, 377 (2003).
[21] A. Pakou and K. Rusek, Phys. Rev. C **69**, 057602 (2004).
[22] E. Vulgaris, L. Grodzins, S. G. Steadman, and R. Ledoux, Phys. Rev. C **33**, 2017 (1986).
[23] K. Rusek, I. Martel, J. Gomez-Camacho, A. M. Moro, and R. Raabe, Phys. Rev. C **72**, 037603 (2005).
[24] A. R. Barnett and J. S. Lilley, Phys. Rev. C **9**, 2010 (1974).
[25] A. J. Koning and J. P. Delaroche, Nucl. Phys. A **713**, 231 (2003).
[26] M. Rodríguez-Gallardo, J. M. Arias, J. Gómez-Camacho, A. M. Moro, I. J. Thompson, and J. A. Tostevin, Phys. Rev. C **80**, 051601(R) (2009).
[27] N. Yu *et al.*, J. Phys. G **37**, 075108 (2010).
[28] S. Santra, S. Kailas, K. Ramachandran, V. V. Parkar, V. Jha, B. J. Roy, and P. Shukla, Phys. Rev. C **83**, 034616 (2011).
[29] S. Santra, P. Singh, S. Kailas, A. Chatterjee, A. Navin, A. Shrivastava, A. M. Samant, and K. Mahata, Phys. Rev. C **60**, 034611 (1999).
[30] N. Keeley, J. M. Cook, K. W. Kemper, B. T. Roeder, W. D. Weintraub, F. Maréchal, and K. Rusek, Phys. Rev. C **68**, 054601 (2003).
[31] T. Aumann *et al.*, Phys. Rev. C **59**, 1252 (1999).